Full-volume characterization of an AGATA segmented HPGe gamma-ray detector using a ^{152}Eu source

B. de Canditiis, G. Duchêne, M.H. Sigward, M. Filliger, F. Didierjean, M. Ginsz, D. Ralet

Full-volume characterization of an AGATA segmented HPGe gamma-ray detector using a 152Eu source.

Journal:	*European Physical Journal A*
Manuscript ID	EPJA-106123.R1
Manuscript Type:	New Tools and Techniques
Pertinent Field:	Experimental
Date Submitted by the Author:	n/a
Complete List of Authors:	De Canditiis, Bartolomeo; IPHC, ; Université de Strasbourg, Duchene, Gilbert; Institut pluridisciplinaire Hubert Curien, DRS Sigward, Marie-Hélène; IPHC Filliger, Michel; IPHC Didierjean, François; IPHC Ginsz, Michael; Mirion Technologies Canberra Ralet, Damian; Mirion Technologies Canberra
PACS:	
Keywords:	Nuclear Physics

Eur. Phys. J. A manuscript No.
(will be inserted by the editor)

Full-volume characterization of an AGATA segmented HPGe gamma-ray detector using a ^{152}Eu source.

B. De Canditiis[1,a], G. Duchêne[1], M.H. Sigward[1], M. Filliger[1], F. Didierjean[1], M. Ginsz[2], D. Ralet[2]

[1]Université de Strasbourg, CNRS, IPHC UMR 7178, F-67000 Strasbourg, France
[2]MIRION Technologies Canberra, 1 chemin de la Roseraie, 67380 Lingolsheim, France

Received: / Accepted:

Abstract Scanning tables use collimated gamma-ray sources to perform full volume characterization of position sensitive detectors. One of such tables is hosted at IPHC Strasbourg. It was designed and built within the AGATA collaboration. It exploits the Pulse Shape Comparison Scanning (PSCS) technique to build databases of pulses used to characterize the response of high purity germanium (HPGe) detectors and perform R&D on such crystals. Ultimately, measured databases could be used by the pulse shape analysis (PSA) algorithms employed in AGATA experiments. The table can perform full volume scans of large volume detectors in short times, with a good spatial resolution and at different energies. Lately, the table was upgraded with a new ^{152}Eu source, which emits gamma rays in cascades of different energies. A scan with such source is performed for the first time. It allows to build different energy databases in one single scan. The present work aims at testing the performances of the PSCS technique with a multi-energetic source and verifying some assumptions of the Shockley-Ramo theorem which are at the base of the PSA algorithms used for gamma-ray tracking arrays.

Keywords HPGe detectors · Full volume characterization · Pulse Shape Analysis (PSA) · AGATA · Scanning table · ^{152}Eu source

1 Introduction

The Advanced GAmma Tracking Array (AGATA) [1, 2] is a new generation array of high-purity germanium (HPGe) segmented detectors. Designed and built in the framework of an European collaboration, it will be composed by 180 large-volume, encapsulated, asymmetric, 36-fold segmented detectors covering a solid angle of $\sim 80\%$ of 4π. Presently, the array is composed by 40 detectors in operation in GANIL [3] and since 2010 the array is used in experiments to study the structure of atomic nuclei as a function of angular momentum, isospin, and temperature.

The main feature of AGATA is the ability to reconstruct the history of the interactions of a gamma ray scattering in the array, which is possible thanks to dedicated tracking algorithms [4–8]. The reconstruction of the gamma-ray trajectories makes obsolete the use of BGO Compton shields. Moreover, it allows a more precise determination of the first interaction which leads to a substantial improvement of the Doppler correction and therefore of the in-beam energy resolution. Tracking also allows the measurement of the linear polarization of gamma rays [9], which is useful for the determination of the parity of the nuclear states of interest.

The first step for the tracking algorithm is to determine the positions of each interaction of the gamma rays in the array. This is performed with pulse-shape analysis (PSA) algorithms [10–16] that, for a given interaction, compares the experimental pulse shape with a database of calculated pulse shapes associated with spatial coordinates within the volume of the detector.

Databases of pulses are presently obtained numerically using the AGATA Detector Library (ADL) [11] leading to good tracking performances. However, some characteristics of the detectors such as the real impurity distribution and the thickness of the dead layers are not always correctly known and their implementation is subject to uncertainties. A novel approach to database construction is the implementation of full volume characterization of the detectors via three-dimensional scans realized with dedicated tools called scanning tables [17–20].

[a]e-mail: bart.decan@gmail.com

A first kind of such tables [17, 18] performs scans of germanium detectors by irradiating them from below with a collimated gamma-ray source. Then the databases are built with the interacting gamma rays that undergo a 90° Compton scattering and that are detected in coincidence by surrounding scintillator crystals, collimated by narrow slits. The double collimation grants to these tables a great geometrical precision (with voxels of about $8mm^3$) at the cost of having a low counting rate due to the imposed coincidence condition ($\sim$ 100 signals in total per point).

A second kind of scanning tables [19, 20] make use of the two $511\,keV$ gamma rays emitted back-to-back from the β^+ decay of a ^{22}Na source to determine precisely the emission direction with an imaging detector. The scanned germanium detector is exposed two times from two orthogonal directions and the database is built by reconstructing off-line the position of crossing interacting gamma rays (voxels of $\sim 8\,mm^3$).

The former technique enables to obtain a $\sim$ 2000 points database of an AGATA detector in about one to two months, whereas the latter performs a full volume scan in few days.

A scanning table, realized within the framework of the AGATA collaboration, is based at the IPHC of Strasbourg [21]. This scanning table is designed to perform three-dimensional scans with a large amount of scanned points and relatively short running times implementing the Pulse Shape Comparison Scan (PSCS) technique [22]. The PSCS technique allows to measure a database by comparing two datasets of pulses obtained by performing two two-dimensional scans, in which the detector is oriented in two different directions perpendicular to each other (e.g. vertical and horizontal). With such technique it is possible to scan an AGATA crystal with a $2\,mm$ pitch in about two weeks, obtaining a database of 45000 to 48000 points depending on the detector geometry (there are four different AGATA crystal geometries). Thus, the IPHC scanning table combines the advantages of both coincidence and imaging scanning tables as it is relatively fast and precise. Moreover, it allows the use of different gamma-ray sources with different energies, leading to versatility in the characterization process as low energies can be used to explore the detector surface while the full volume can be scanned at higher energies.

Currently, three collimated sources are available for the scans. Sources of ^{241}Am and ^{137}Cs were already tested with the scanning table [21, 23]. Recently a new ^{152}Eu source was acquired. As the source emits gamma-rays with different energies, this opens the possibility to characterize the detector response at different energies with just one scan. A three-dimensional scan of a symmetrical AGATA (S-type) detector was performed using the ^{152}Eu source and five different-energy databases were built. This unique measurement is performed for the first time and it aims to explore the new technique and to verify, by comparing the different energy databases, that the pulse shapes are independent of the energy of the gamma ray interaction that generates them. This principle asserted by the Shockley-Ramo theorem [24–26] is at the base of the AGATA PSA algorithms implementation but has never been demonstrated experimentally. In the first part of this paper the experimental setup is described. Subsequently, the data treatment is discussed followed by the experimental results. Conclusions and perspectives are given in the last section.

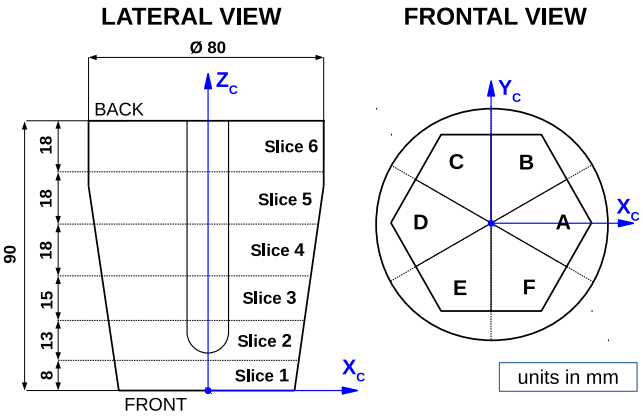

Fig. 1: Dimensions of the S001 detector (units in mm). The figure shows the numbering of the slices (1 to 6, on the left) and the labeling of the sectors (A to F, on the right) in which the detector is segmented. The blue lines show the reference frame used in the following discussion for PSCS technique results presentation.

2 Experimental setup

2.1 S001 detector unit

The measurements described in this work are realized on the S001 AGATA detector unit which is a 36-fold segmented, closed-end, coaxial, n-type HPGe crystal with a tapered hexagonal geometry and a symmetric shape (S-type) [27, 28]. The crystal geometry and its segmentation are represented in figure 1 and described in detail in reference [29].

From the detector, 36 segment signals plus 1 total-energy signal are collected, the former on the boron segmented contacts and the latter on the central contact

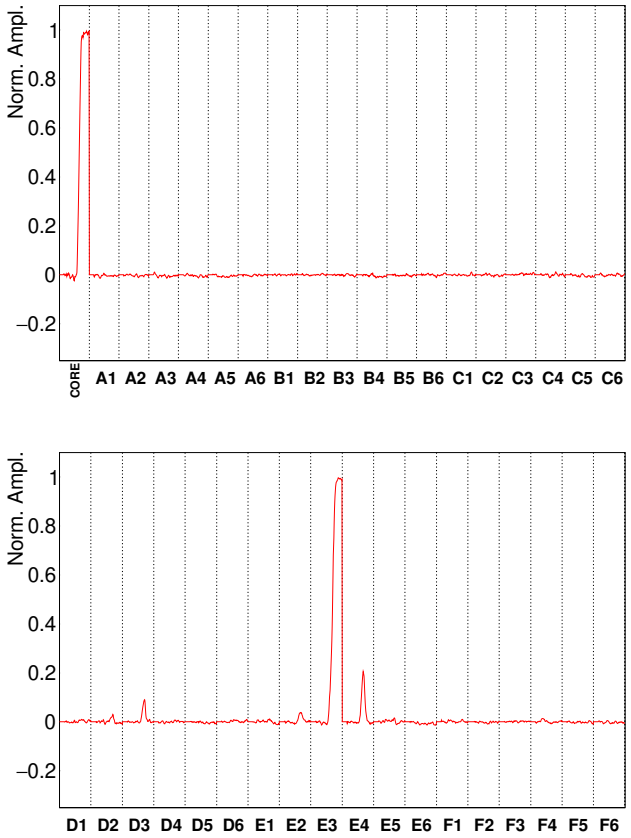

Fig. 2: Example of signals coming from a S-type AGATA detector plotted as a supertrace (see text for details).

(core). The signals are collected by 37 charge-sensitive preamplifiers [1, 30–32] characterized by low noise performances, large dynamic range for energy detection ($0 - 5.7\,MeV$ or $0 - 20\,MeV$) and fast response time of $\sim 25\,ns$. A large bandwidth ensures good resolution for pulse-shape analysis and good timing properties.

Figure 2 shows an example of a signal generated by a $662\,keV$ gamma ray (^{137}Cs source) interacting in segment E3. The signal is presented as a supertrace, defined as a compact, continuous representation of all the leading edges coming from the 36 segments and the core of the detector. The signal is normalized with respect to the core signal amplitude. The signals corresponding to the core segment and the hit segment are defined as net charge signals, while the signals corresponding to other segments are called transient signals. The shapes of the net charge and transient signals depend on the position where the interactions take place, thus giving the detector position-sensitive properties.

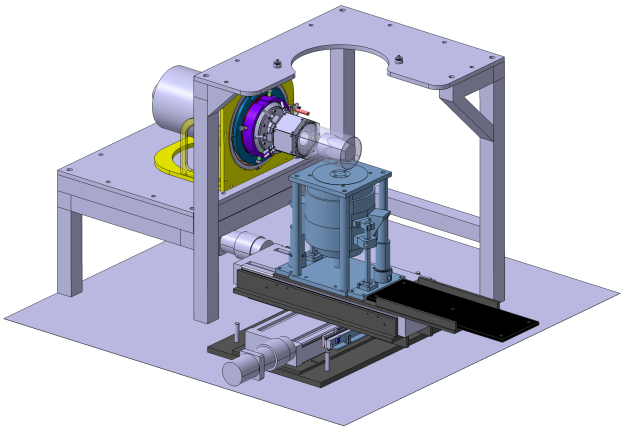

Fig. 3: Schematic view of the scanning table.

2.2 The PSCS technique and the IPHC scanning table

The PSCS technique [22, 29] allows to characterize the full volume of a position sensitive detector, such as the S001 unit. This is done by irradiating the detector from two different positions with a collimated gamma-ray source. The detector is put at first in vertical position and irradiated at different points with a given step forming a regular vertical grid. For each point a dataset of pulses generated along the gamma-beam direction is acquired. The detector is then put in horizontal position and the procedure is repeated ensuring that the horizontal grid intersects the vertical grid. Subsequently, a χ^2 algorithm (later described in section 3) selects the most similar pulse shapes of two given intersecting datasets, that is the ones that are generated by the interactions happening around the intersection point. The algorithm is applied to all the couples of intersecting datasets and a database of pulses is created.

The technique above described is implemented by the IPHC scanning table [21, 23, 28], shown in figure 3, which was designed with the aim of performing scans in short times, with good spatial resolution and variable energies.

The table is formed by two metallic plates that hold the detector in vertical or horizontal position. The detector is actually placed in an adjustment frame that allows precise alignment on the table. Underneath, a cylindrical, metallic collimator sits on two motorized axes that allows its planar movement. The central part of the collimator is swappable allowing to choose collimation diameters of $1\,mm$, $0.5\,mm$ and $0.2\,mm$. The collimator can be opened from below allowing the insertion of three source capsules. The characteristics of these sources are given in table 1.

Table 1: Characteristics of the sources used by the IPHC scanning table. Branching ratios (BR) are found at [33]. The BR of the ^{152}Eu source are normalized with respect the total BR of the branches with the highest decay probability. The three sources have cylindrical shape. The dimension of the ^{241}Am and ^{137}Cs sources are $3\,mm$ for both the diameter and height. The ^{152}Eu has a $3.2\,mm$ diameter and a $2.3\,mm$ height.

Source	Activity(GBq)	E_γ(keV)	BR
^{241}Am	1.5	60	0.36
^{137}Cs	1.85	662	0.851
^{152}Eu	0.74	122	0.286
		245	0.076
		344	0.265
		779	0.129
		1408	0.210

The data acquisition is done with TNT2 cards [34], developed at IPHC. These cards cover both the digitizing and pre-processing of the signals done by the standard AGATA electronics [1]. As each card has 4 channels, 10 cards are used for scanning an AGATA detector unit, 9 for the 36 segments and one for the core signal used as trigger. Each channel samples the incoming signal with $14\,bit$ resolution and $100\,MHz$ rate. Subsequently, the energy is measured applying a moving window deconvolution algorithm [35, 36]. For the measurements shown in this work, the signals were sampled in a time window of $1.2\,\mu s$ (120 samples) and a $5.95\,\mu s$ shaping time was used for the moving window deconvolution algorithm [28].

3 Data acquisition and treatment

3.1 Performed scans

Before proceeding with the scans, the detector is aligned on the scanning table by performing several preliminary scans and precise adjustments. The alignment ensures that the measured tilt of the detector, with respect to the reference frame of the scanning table, is at maximum 0.05°. A detailed description of the general alignment procedure can be found in [21, 23, 28].

For the work here presented, two three-dimensional scans of the S001 detector were performed with the ^{137}Cs and ^{152}Eu sources. Both scans were performed with a pitch of $2\,mm$ and the $1\,mm$ diameter collimator. The ^{137}Cs scan had a duration of 2.5 minutes per point, leading to a total duration of 6.7 days (2.5 days for the vertical acquisition and 4.2 days for the horizontal acquisition, including the nitrogen refill pauses). As the PSCS technique using a ^{137}Cs source has been already tested and validated [21, 23], this scan is used as a reference.

The acquisition times for the ^{152}Eu scan, instead, were significantly longer due to the fact that the source intensity ($0.74\,GBq$) is 2.5 times lower than the one of the ^{137}Cs source ($1.85\,GBq$) and is divided among its different emitted gamma rays. Among the peaks of interest for the analysis ($122\,keV$, $245\,keV$, $344\,keV$, $779\,keV$ and $1408\,keV$ all gated in a $\pm 2\,keV$ window) the $779\,keV$ has one of the lowest branching ratio. In order to obtain similar statistics between the events at this energy and the ones at $662\,keV$, an acquisition time of 60 minutes per point was used. To lower the global scanning times, only one single sector (sector B) was scanned. Nevertheless, the total scan duration was 54 days (14 days for the vertical acquisition and 40 days for the horizontal acquisition, including the nitrogen refill pauses).

The ^{152}Eu events, which are acquired in a single scanning procedure, are sorted and prepared in five separated datasets, one for each energy, and treated independently by the χ^2 selection algorithm, described in section 3.2, leading to the construction of five different databases. For each dataset, only 1-fold events are selected, that is the events in which a gamma ray interacts in a single segment. Moreover, the pulse shapes coming from each segment are normalized and then aligned to their T^{50}, the time at which the pulses reach 50% of their maximum amplitude. In particular the transient pulses are normalized and aligned with respect to the signal of the hit segment.

For the $245\,keV$ and $344\,keV$ databases, data from the last slice of the detector (slice 6) was not taken into account. In fact, it is observed that the peak to total ratio relative to these energies drops below 70% [28] towards the back of the detector. The same considerations are applied to the $122\,keV$ database and only the data in the first two slices of the detector (slice 1 and 2) are considered. Finally, figure 1 shows the reference frame in which the results of the analysis will be presented.

3.2 The χ^2 algorithm

The acquired datasets are processed with a code that implements the pulse-shape comparison algorithm. The comparison between two pulses is performed by calculating the χ^2 value with equation

$$\chi^2 = \frac{\sum_{seg\in\mathcal{M}} \sum_{i=i_0}^{i_f} (v_{seg,i} - h_{seg,i})^2}{M \cdot (i_f - i_0)} \quad (1)$$

where *seg* is the segment index, $\mathcal{M}$ is the M dimensioned ensemble of segments formed by the Core seg-

ment, the hit segment and the neighboring segments of the hit segment (4 segments if the hit segment is in the middle of the detector or 3 segments if the hit segment is at the top or bottom of the detector) and v_i and h_i are the samples of the vertical and horizontal signals, respectively. Finally, the comparison is performed on a subset of samples in the window $[i_0, i_f]$ containing the leading edge of the pulse.

Only the signals produced by events happening in the same segment are compared. Each pair of events compared is inserted in a χ^2-value-ordered list. For a given point, the number of pulses in the compared vertical and horizontal sets are typically of the order of $\sim 10^3$ (this number depends on the detector geometry and on the relative source position), leading to about $\sim 10^6$ couples of pulses. To ensure both a strict selection and sufficient statistics, at the end of the procedure only the 200 couples with the lowest χ^2 values are selected. Among these, some events may have been selected more than once. The duplicates are discarded from the list before the mean pulse-shape refinement is applied. This procedure (described in detail in [29]) uses again the pulse-shape comparison to reject the most diverging pulses, with respect to the average pulse, giving a more coherent final selection of events. About 140 pulses are finally selected for each coordinate of the pulse shape database.

The remaining pulses are re-aligned and averaged following the so-called difference minimization algorithm (see section 5.3.2 of reference [37]) and the resulting pulse is inserted in the database. The algorithm acts as follows. A first signal is aligned to a fixed point. Subsequently, each other signal is shifted and compared to the first one by calculating the root mean square (RMS) difference. The RMS is calculated in the T_{10}^{90} time window (defined as the time interval in which the amplitude of the considered signal goes from 10% to 90% of its maximum amplitude) of the signal. Although, in the case of the $122\,keV$ database the RMS is calculated in the T_{25}^{90} time window due to lower signal to noise ratio. The shift relative to the minimum RMS is then used as the new alignment point for the signal. All the so aligned signals are then averaged and the procedure is repeated using this preliminary mean signal as the first signal. At the end of the procedure a new average signal is calculated and the resulting pulse is inserted in the database.

Once the database is created, it is important to note that some pulses calculated by the algorithm are associated to points that lay outside the volume of the detector. Such cases can exist because the χ^2 selection algorithm is blind of the geometry of the detector. Since on average the χ^2 values associated to these pulses is higher than the χ^2 values of the pulses selected inside the detector, it is possible to set a threshold in order to filter them and clean the database.

The overall procedure is resumed by the following steps:

1. Two intersecting datasets, corresponding to a given detector coordinate, are selected and their pulse shapes are compared through a χ^2-like formula:
2. The 200 best-matching couples are selected.
3. Duplicate events are rejected.
4. The remaining pulses are treated with the mean pulse-shape refinement. ~ 140 pulses are finally selected.
5. The pulses are re-aligned and averaged with the difference minimization algorithm.
6. Steps 1 through 5 are repeated until completion of the database.
7. The database is cleaned from unphysical points.

4 Experimental results

4.1 Comparison of databases of different energies

As a first test, the $662\,keV$ and $779\,keV$ databases are compared, since they are close in energy. It is possible to make a first comparison of the two databases by looking at the distribution of parameters such as the T_{10}^{90} and the left/right image charge anisotropy ($ICA_{l/r}$) which both depend from the shape and characteristics of the considered signals. The T_{10}^{90} is defined as above (section 3.2) and the left/right ICA is defined as [23]

$$ICA_{l/r} = \frac{I_l - I_r}{I_l + I_r} + 1 \tag{2}$$

where I_l and I_r are the integrals of the transient signal of the left and right neighboring segments. The $+1$ is an offset to make the ICA value range in [0,2]. The ICA parameter give an indication on the location of the interaction relative to the neighboring segments. The distributions of the T_{10}^{90} and $ICA_{l/r}$ values are shown in figures 4 and 5 for both the $662\,keV$ and the $779\,keV$ databases. Distributions at three database slices ($Z_C = 6\,mm$, $48\,mm$, and $80\,mm$) are presented. They are very similar, hinting that the two scans are comparable.

Indeed, if two pulses with the same coordinates are compared, as in figure 6, it can be seen that they are almost identical as it is shown by the residual values between the two traces (in green). In the example shown in figure 6 the maximum residual value among the two supertraces is $\sim 0.8\%$ of the maximum amplitude reached by the net charge signal. As the maximum residual value is a tool that quantify the maximum amplitude difference of two given pulses, it can be used as an index

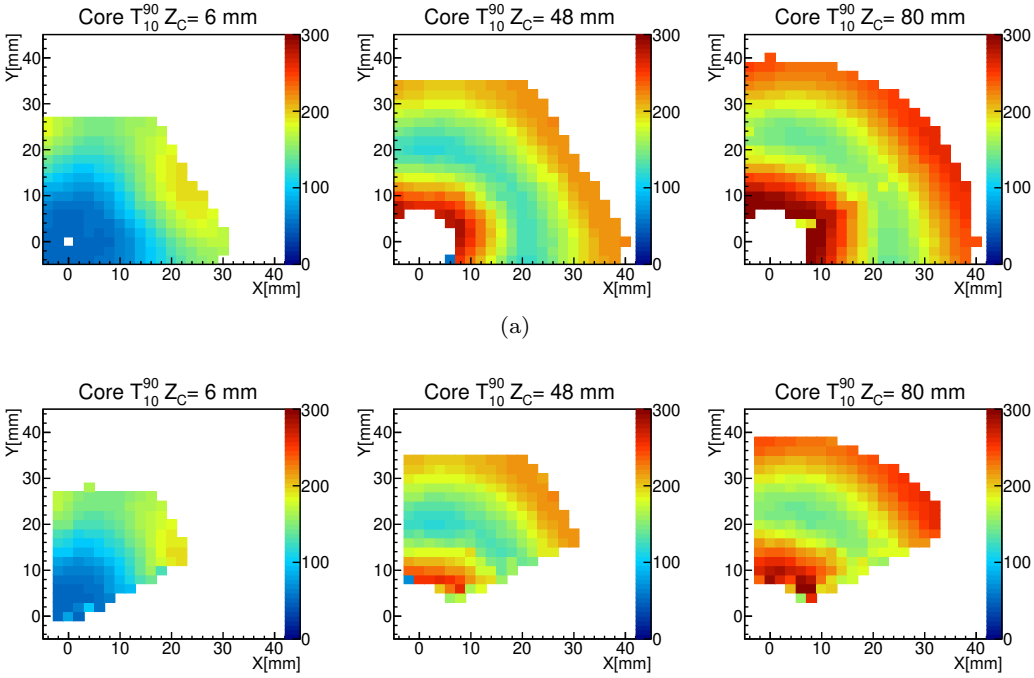

Fig. 4: Distributions of the T_{10}^{90} in three slices of (a) the $662\,keV$ database (the histograms include part of sector A and sector B) and (b) the 779 keV database (sector B). The color scale is in nanoseconds. The $2\,mm$-thick (1 grid unit) slices considered are at $Z_C = 6\,mm$, $48\,mm$ and $80\,mm$.

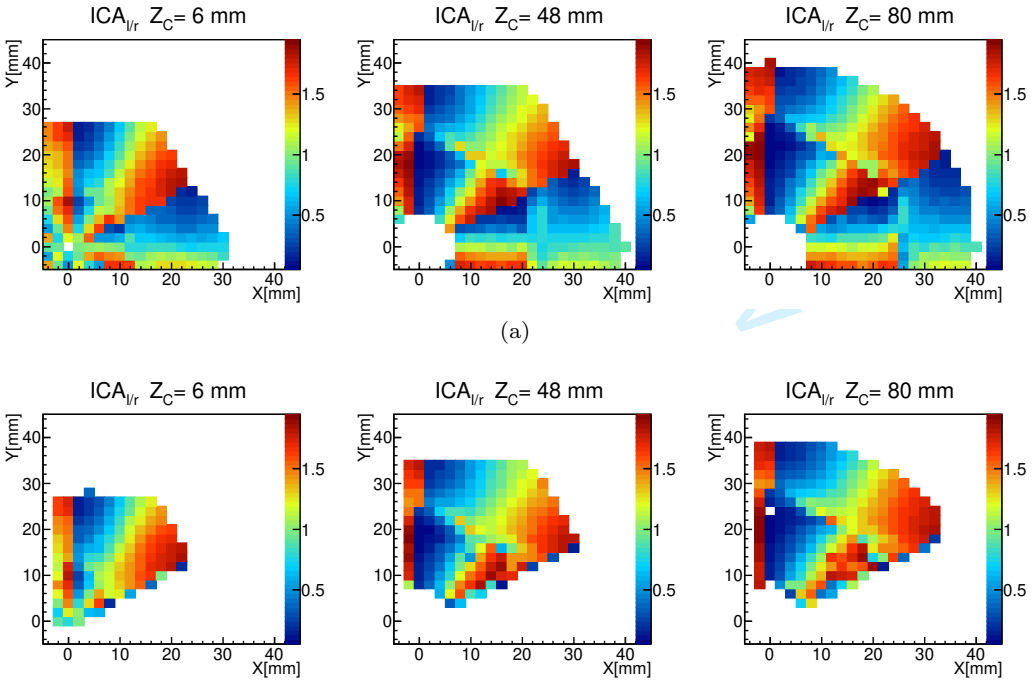

Fig. 5: Distributions of the $ICA_{l/r}$ in three slices of (a) the $662\,keV$ database (the histograms include part of sector A and sector B) and (b) the 779 keV database (sector B). The $2\,mm$-thick (1 grid unit) slices considered are at $Z_C = 6\,mm$, $48\,mm$ and $80\,mm$.

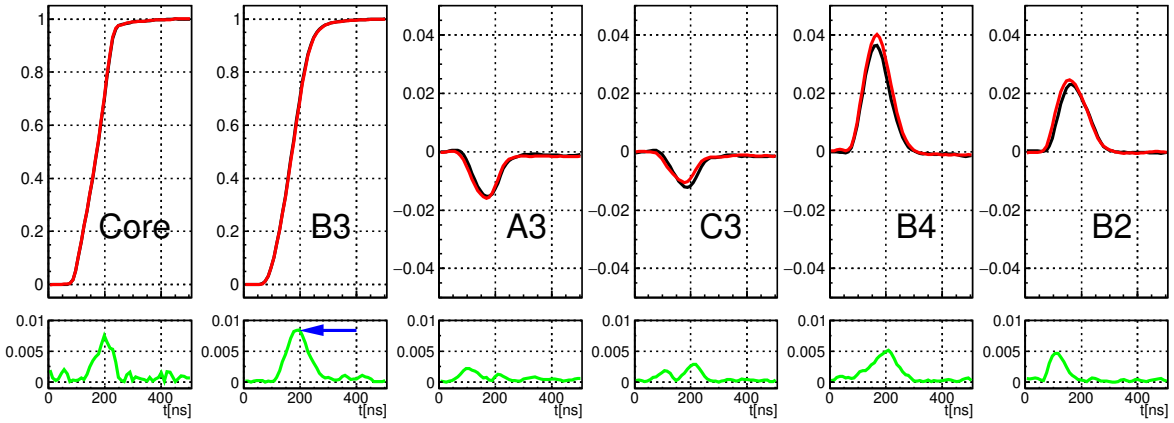

Fig. 6: Comparison of two pulse shapes taken at the same point ($X_C = 10\,mm$, $Y_C = 20\,mm$, $Z_C = 30mm$) of the $662\,keV$ database (black line, upper panels) and $779\,keV$ database (red line, upper panels). The green lines in the lower panels show the residual value between the two pulses. The blue arrow shows the residual with the maximum value.

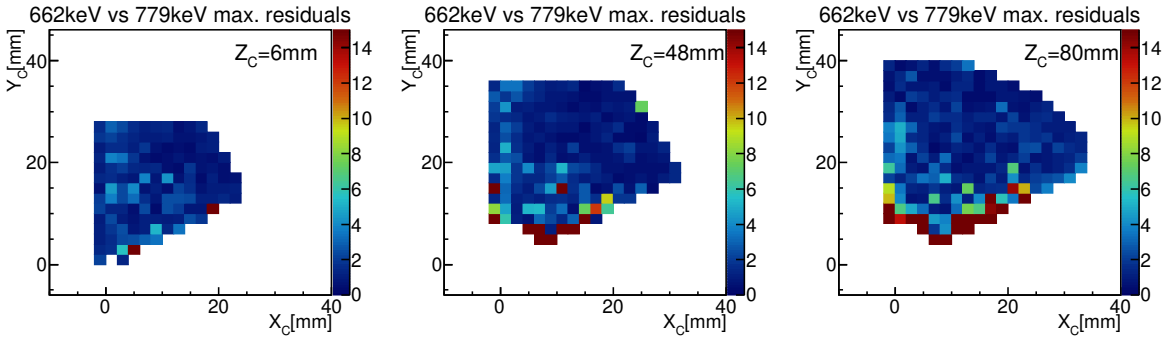

Fig. 7: Distributions of the maximum residuals (see text and figure 6), in percent of the full energies, between the pulses of the $662\,keV$ and $779\,keV$ databases. The data are relative to the $2\,mm$-thick (1 grid unit) database slices at $Z_C = 6\,mm$, $48\,mm$ and $80\,mm$.

to observe where and how much two databases diverges the most. Thus, the comparison can be extended to all the points of the $662\,keV$ and $779\,keV$ databases. The distributions of the maximum residuals, in percent, for three database slices are shown in figure 7. The distributions are quite homogeneous in each slice despite some points having high values (dark red) which appear to be concentrated near the core contact and the segmentation lines.

The average value for each database slice can be calculated and the results plotted as a function of Z_C as in figure 8a (red markers). The graph shows that the average maximum residual per database slice has a value of 2% to 3% toward the front of the detector and increases slightly towards the back of the crystal where it reaches values up to 6% at the back. Moreover, in correspondence of the segment separation surfaces ($Z_C = 14\,mm$, $22\,mm$, $36\,mm$, $56\,mm$ and $74\,mm$) slight value increases are observed. The same analysis is performed by taking into account only the transient pulses. The graph, in figure 8b, shows that the average maximum residual between transient pulses is lower with respect to the net charge signals, ranging in the interval 1% to 3%. The bars in figures 8a and 8b show the standard deviation of the maximum residual distribution for database slices at the front, center and back of the detector. They show a quite large spread, mostly due to single or clusters of points which exhibit large values (as seen in figure 7). These points are mostly concentrated along the segmentation surfaces, where it has been observed [28, 29] that the PSCS technique presents some limitations.

The above analysis is performed comparing the remaining measured databases in pairs. At first, the $1408\,keV$ database is compared with the $662\,keV$ and $779\,keV$ databases. The results are represented in figure 8 (blue

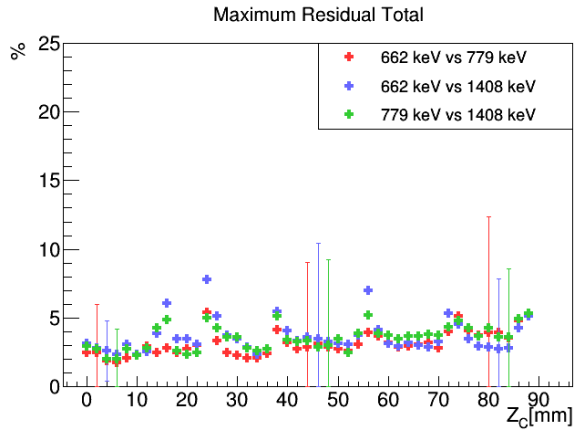

(a)

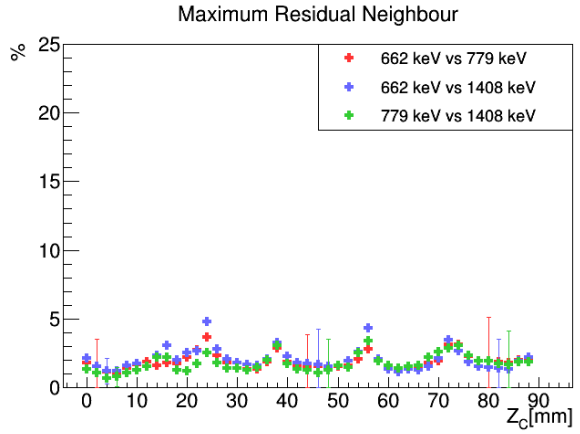

(b)

Fig. 8: Average maximum residual, as a function of Z_C. Each point represents the mean value of the maximum residual distribution corresponding to a given database slice (see figure 7). The graphs refers to the comparison, pair by pair, between the $662\,keV$, $779\,keV$ and $1408\,keV$ databases. In (a) the maximum residuals are calculated with the whole supertrace while in (b) only the transient pulses are used.

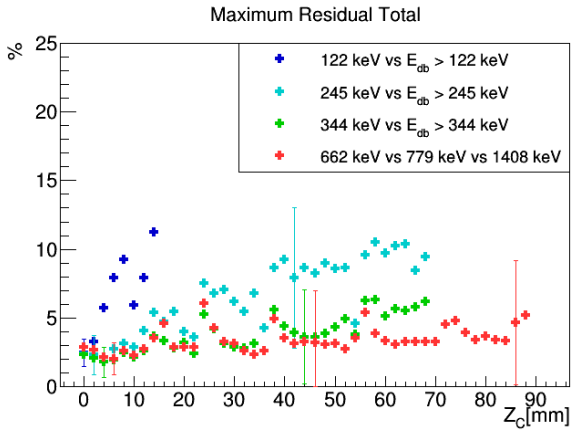

(a)

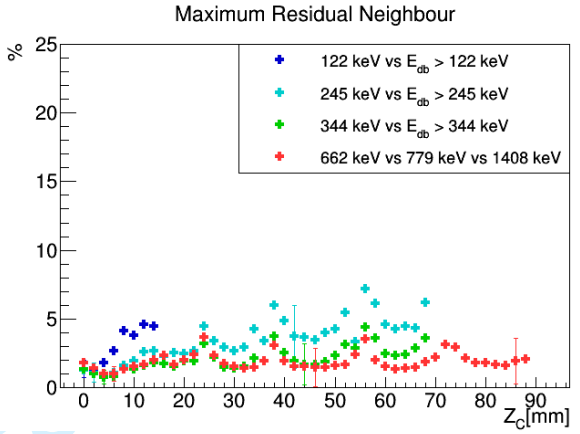

(b)

Fig. 9: Average maximum residual, as a function of Z_C. Each point represents the mean value of the maximum residual distribution corresponding to a given database slice (see figure 7). The graphs refers to the comparison, pair by pair, between the $122\,keV$, $245\,keV$, $344\,keV$ $662\,keV$, $779\,keV$ and $1408\,keV$ databases. The data series corresponding to the comparison between a database of a given energy and all the databases of higher energy are regrouped and averaged (see text for detail). In (a) the maximum residuals are calculated with the whole supertrace while in (b) only the transient pulses are used.

and green markers, respectively) and show a similar trend, with comparable values, of the average maximum residuals, with respect to the $662\,keV$ and $779\,keV$ compared databases.

Due to their similarity, the three graphs are grouped in a single, average data series and reported with red markers in figure 9. The same operation is performed for the data series corresponding to the comparison between the database of a given energy with the ones of higher energy (i.e. $344\,keV$ versus $662\,keV$, $779\,keV$ and $1408\,keV$). It is, in fact, observed that these data series are comparable as seen for the previous case (i.e. comparison among databases with energies larger than $500\,keV$). This choice is taken mainly to ease the readability of the results, represented in figure 9.

The data series relative to the $344\,keV$ database (green markers) follow the same trend of the high end energy ones until $Z_C = 46\,mm$. From there on, the $344\,keV$ database and the high end energy databases start to diverge. For $Z_C > 56\,mm$ the average maximum residuals reach values around 7% , which is more than a factor 2 larger than the ones for the high end energy data series.

Similarly, the $245\,keV$ database is comparable with all the databases with $E_\gamma > 245\,keV$ (light blue markers) in the first two slices of the detector ($Z_C < 24\,mm$) then it starts to diverge reaching values for the average maximum residuals which are over 10% towards the back of the detector.

Finally, the blue markers in figure 9 show the comparison between the $122\,keV$ and the other energy databases. These data series don't follow any of the trends previously discussed as the total average maximum residuals have values of $\sim 5\%$ in the front slice of the database and then increase to over 10% toward slice 2 of the detector.

4.2 Discussion

The analysis presented above indicates that, for gamma-ray energies larger than $500\,keV$, the pulse shapes are independent of the energy of the interaction. The corresponding databases match, in average, within 3% with maximum values around 5%. For energies lower than $500\,keV$ discrepancies appear. The $344\,keV$ and $245\,keV$ databases follow the same trend of high energy databases until $Z_C = 46\,mm$ and $Z_C = 24\,mm$ respectively, while the $122\,keV$ database presents overall large inconsistencies.

The observed discrepancies for energies below $500\,keV$ are not a prove that the pulse shapes differ with the energy of the interacting gamma-ray. They may rather be related to limitations of the pulse-shape selection and to the PSCS implementation, especially when approaching segmentation or segment slice borders.

As a first hypothesis one can think that the discrepancies are due to the gamma-ray absorption that lowers the statistics of vertical datasets. However, this alone can't be the cause of the phenomenon. In fact, by analyzing the events distribution per slice of the vertical datasets it can be seen that the available statistics for the back slices of the detector is larger for the $344\,keV$ scan with respect to the $779\,keV$ and $1408\,keV$ ones [28]. This is due to the higher branching ratio of the $344\,keV$ gamma ray which compensates for the absorption in the germanium.

Another factor that can cause discrepancies is the noise level of the pulses used for the χ^2 selection. For example, the noise amplitude of the $122\,keV$ pulses is measured [28] to be in average $\sim 5\,keV$ and $\sim 2\,keV$ for the core and segment contacts, respectively, which correspond to $\sim 6\%$ and 2% of their maximum amplitude. The transient signals amplitudes are generally small with respect to the amplitude of the net charge signal. In fact, apart from the segment border where they may rise up to $\sim 30\%$, they are generally limited to $\sim 15 - 10\%$, or less, of the net charge signal amplitude. These amplitudes are to be compared with the 2% noise amplitude, which therefore certainly affect the pulse shape as shown in figure 10. Such distortion can influence the χ^2 selection. High levels of noise can also lead the time alignment to fail as the T^{50} value can be incorrectly shifted due to the noise and the χ^2 selection would then be performed on events that are not properly aligned.

The analysis evidenced that the larger discrepancies between signals are found on the net charge signals rather than on the transient signals (figure 9). It has to be noticed, however, that the transient signals are normalized to the maximum amplitude of the net charge signals. Since the amplitude of transient signals is in relation smaller, it may mean that actually the difference between the transient pulses has a more relevant impact on the database comparison.

Finally, it should be mentioned that effects due to the energy of the detected interaction were observed and analyzed in [38]. In that work, in-beam events acquired with the first AGATA triple cluster (3 crystals) were reconstructed with the PSA and tracking algorithms used for on-line data treatment and off-line data analysis. The results showed that the spatial resolution improves linearly in the range $\sim 250\,keV$ to $1500\,keV$ as the energy increases and remains constant at higher energies. Although a simple, direct comparison among the results shown in the present work and the ones in [38] is not possible, it is worth to note that the AGATA PSA algorithm uses a similar factor of merit formula to the one used for the PSCS technique (see equation 1) with an optimized exponent. Thus, it is expected that the PSA algorithm may present problems similar to the PSCS ones for events which energies are below $500\,keV$ and may be less and less precise with decreasing energy. This phenomenon may partially explain the spatial resolution deterioration at low gamma-ray energy evidenced in [38].

5 Conclusions and Perspectives

Three-dimensional scans were performed with the ^{137}Cs and ^{152}Eu sources. Due to the low activity of the source and the branching ratio of the transitions of interests, the ^{152}Eu scan was restricted to one sector of the detector (sector B). The ^{152}Eu scan allowed to construct five different databases of pulses, with different energies and at exactly the same points, in a single measurement. Databases were built for the energies $122\,keV$, $245\,keV$, $344\,keV$, $779\,keV$, $1408\,keV$ (^{152}Eu) and $662\,keV$ (^{137}Cs).

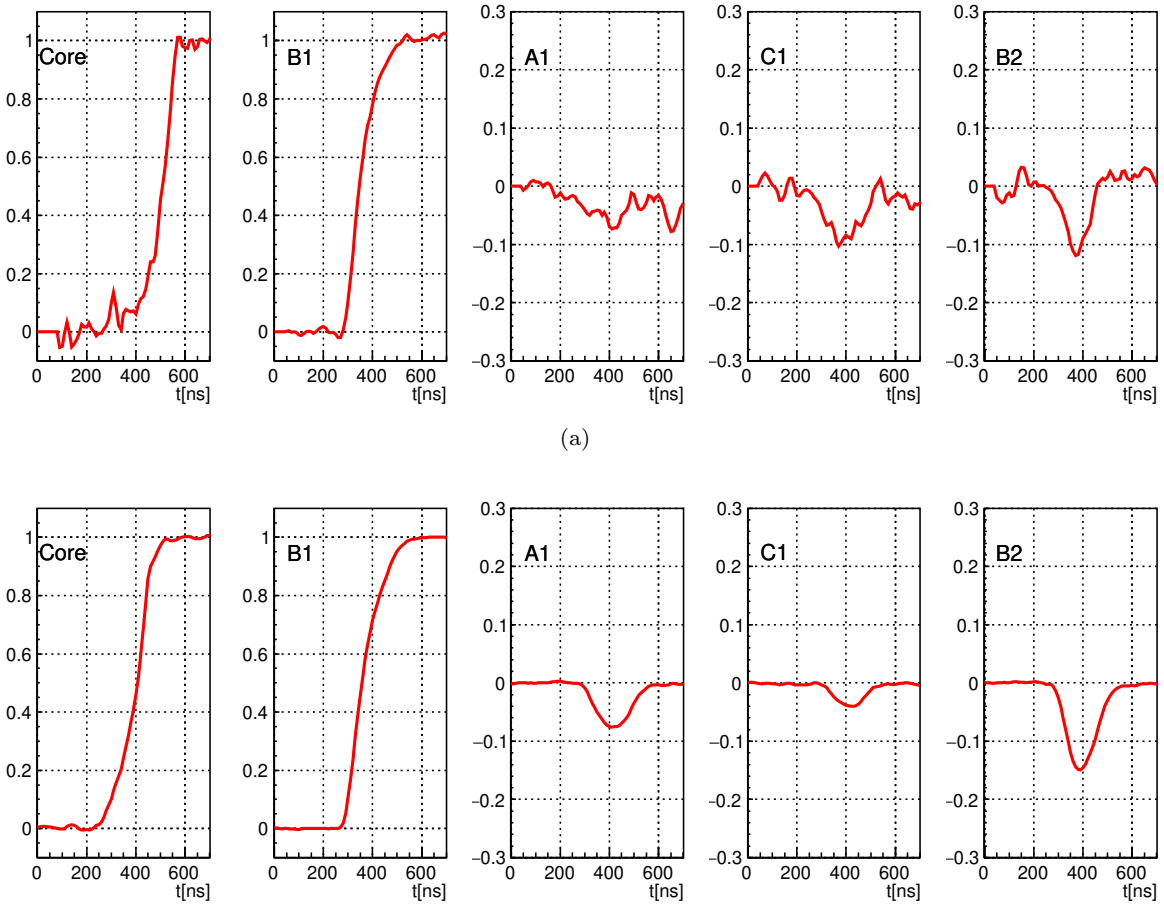

Fig. 10: Examples of pulses used for the χ^2 selection interacting in segment B1. The pulse shown in (a) and (b) are relative to the 122 keV and 1408 keV datasets, respectively. The noise in the 122 keV signal is non-negligible, especially for the transient signals, while it has no influence on the 1408 keV signal.

A comparison was made within each database, and the maximum residual value between two signals associated to the same point of the database was chosen as comparison parameter. The databases with an energy $> 500\,keV$ proved to be comparable within each other, with differences varying along the crystal length from around 3% (front) up to 5% (back), in average. Some discrepancies were instead found with the 344 keV database for Z_C values larger than 46 mm. The residual values appeared to diverge by a factor 2 towards the back of the detector. The same behavior was found for the 245 keV database which starts to diverge for Z_C values larger than 24 mm. Finally, the 122 keV database proved to be strongly divergent from the other databases.

It was supposed that the reasons behind these divergent behaviors are to be attributed to the PSCS technique that somehow is not efficient at low energies. It is hypothesized that the major cause for this lays in the noise level which, for low amplitude signals, can have an impact on the pulse alignment and can distort the transient signals, leading to a loss of information. The impact of the gamma ray absorption on the input statistics was also considered among the discrepancies causes, although this may have only a minor impact.

It was remarked that the parameters shown in the present work share a similar trend to the spatial resolution of the AGATA detectors which deteriorates as the energy of the interacting gamma ray decreases, as observed in [38]. This points out that the PSA algorithms may be less precise for interaction energies below 500 keV. Further investigations on the phenomenon are necessary.

Some improvements on the PSCS technique could lead to better performances. For example, the use of noise filtering techniques, such as the Fourier transform noise canceling, could be evaluated, especially for low energy pulses where the PSCS appears to be more affected. In order to enable measurements with low en-

ergies in a full sector volume using the ^{152}Eu source, a horizontal-horizontal scanning configuration could be tested. It would reduce statistics issues for low energy gamma-ray beams towards the back of the detector.

Finally, as a further analysis, it would be interesting to compare the databases obtained by the IPHC scanning table with the ones measured with other scanning tables exploited by the AGATA collaboration by using the same capsule mounted in a given test cryostat moved from one place to the others. Such measurement is foreseen in the near future.

Acknowledgements This work has been supported by the MIRION Technologies Canberra Company under the contract No 152521 and the OASIS ANR grant under the contract ANR-17-CE31-0026-02.

References

1. S. Akkoyun, et al. AGATA - Advanced GAmma Tracking Array. *Nuclear Instruments and Methods in Physics Research Section A: Accelerators, Spectrometers, Detectors and Associated Equipment*, 668:26 – 58, 2012.
2. A. Korichi and T. Lauritsen. Tracking gamma rays in highly segmented HPGe detectors: A review of AGATA and GRETINA. *The European Physical Journal A*, 55(7):121– 151, 2019.
3. E. Clément, et al. Conceptual design of the AGATA 1π array at GANIL. *Nuclear Instruments and Methods in Physics Research Section A: Accelerators, Spectrometers, Detectors and Associated Equipment*, 855:1 – 12, 2017.
4. J. van der Marel and B. Cederwall. Backtracking as a way to reconstruct compton scattered -rays. *Nuclear Instruments and Methods in Physics Research Section A: Accelerators, Spectrometers, Detectors and Associated Equipment*, 437(2):538 – 551, 1999.
5. A. Lopez-Martens, et al. Gamma-ray tracking algorithms: a comparison. *Nuclear Instruments and Methods in Physics Research Section A: Accelerators, Spectrometers, Detectors and Associated Equipment*, 533(3):454 – 466, 2004.
6. G. Suliman and D. Bucurescu. Fuzzy clustering algorithm for gamma ray tracking in segmented detectors. *Romanian Reports in Physics*, 62:27–36, 2010.
7. F. Didierjean, et al. The Deterministic Annealing Filter: A new clustering method for gamma-ray tracking algorithms. *Nuclear Instruments and Methods in Physics Research Section A: Accelerators, Spectrometers, Detectors and Associated Equipment*, 615:188–200, 2010.
8. S. Tashenov and J. Gerl. Tango - new tracking algorithm for gamma-rays. *Nuclear Instruments and Methods in Physics Research Section A Accelerators Spectrometers Detectors and Associated Equipment*, 622:592–601, 2010.
9. P. G. Bizzeti, et al. Analyzing power of AGATA triple clusters for gamma-ray linear polarization. *The European Physical Journal A*, 51(4):49–60, 2015.
10. R. Venturelli. and D. Bazzacco. Adaptive grid search as pulse shape analysis algorithm for gamma-tracking and results. *LNL Annual Report*, page 220, 2004.
11. B. Bruyneel, et al. Pulse shape analysis and position determination in segmented HPGe detectors: The AGATA detector library. *The European Physical Journal A*, 52(3):70–80, 2016.
12. L. Mihailescu. *Principles and Methods for gamma ray tracking with large volume Germanium Detectors*. Ph.D. thesis, University of Bonn, 2000.
13. L. Mihailescu, et al. The influence of anisotropic electron drift velocity on the signal shapes of closed-end HPGe detectors. *Nucl. Instrum. Meth. A*, 447:350–360, 2000.
14. P. Medina, et al. A simple method for the characterization of HPGe detectors. *Conference Record - IEEE Instrumentation and Measurement Technology Conference*, 3:1828 – 1832 Vol.3, 2004.
15. M. Schlarb, et al. Pulse shape analysis for gamma-ray tracking (Part I): Pulse shape simulation with JASS. *The European Physical Journal A*, 47(10):132–155, 2011.
16. I. Mateu, et al. Simulation of the charge collection and signal response of a HPGe double sided strip detector using MGS. *Nuclear Instruments and Methods in Physics Research A*, 735:574–583, 2014.
17. M. Dimmock, et al. Validation of Pulse Shape Simulations for an AGATA prototype detector. *Nuclear Science, IEEE Transactions on*, 56:2415 – 2425, 2009.
18. T.M.H. Ha, et al. New setup for the characterisation of the AGATA detectors. *Nuclear Instruments and Methods in Physics Research Section A: Accelerators, Spectrometers, Detectors and Associated Equipment*, 697:123 – 132, 2013.
19. N. Goel, et al. Spatial calibration via imaging techniques of a novel scanning system for the pulse shape characterisation of position sensitive HPGe detectors. *Nuclear Instruments and Methods in Physics Research Section A: Accelerators, Spectrometers, Detectors and Associated Equipment*, 652(1):591 – 594, 2011. Symposium on Radiation Measurements and Applications (SORMA)

XII 2010.
20. A. Hernandez-Prieto, et al. Study of accuracy in the position determination with SALSA, a gamma-scanning system for the characterization of segmented HPGe detectors. *Nuclear Instruments and Methods in Physics Research Section A: Accelerators, Spectrometers, Detectors and Associated Equipment*, 823:98 – 106, 2016.
21. M.H. Sigward, et al. Pulse-Shape Comparison Scan of germanium detectors using the IPHC scanning table. To be published.
22. F.C.L. Crespi, et al. A novel technique for the characterization of a HPGe detector response based on pulse shape comparison. *Nuclear Instruments and Methods in Physics Research Section A: Accelerators, Spectrometers, Detectors and Associated Equipment*, 593(3):440 – 447, 2008.
23. M. Ginsz. *Characterization of high-purity, multi-segmented germanium detectors*. Ph.D. thesis, University of Strasbourg, 2015. `http://www.theses.fr/2015STRAE047`.
24. W. Shockley. Currents to conductors induced by a moving point charge. *Journal of Applied Physics*, 9:635–636, 1938.
25. S. Ramo. Currents induced by electron motion. *Proceedings of the I.R.E.*, 27:584–585, 1939.
26. Zhong He. Review of the Shockley-Ramo theorem and its application in semiconductor gamma-ray detectors. *Nuclear Instruments and Methods in Physics Research Section A: Accelerators, Spectrometers, Detectors and Associated Equipment*, 463(1):250 – 267, 2001.
27. J. Simpson, et al. AGATA Technical Design Report. Technical report, 2008.
28. B. De Canditiis. *3D characterization of multi-segmented HPGe detectors. Simulation and validation of the PSCS technique and its application for different energies with a ^{152}Eu source*. Ph.D. thesis, University of Strasbourg, 2020. `http://www.theses.fr/2020STRAE008`.
29. B. De Canditiis and G. Duchêne. Simulations using the pulse shape comparison scanning technique on an AGATA segmented HPGe gamma-ray detector. *The European Physical Journal A*, 56(10):276, 2020.
30. A. Pullia, et al. An advanced preamplifier for highly segmented germanium detectors. *IEEE Transactions on Nuclear Science*, 53(5):2869–2875, 2006.
31. F. Zocca, et al. A time-over-threshold technique for wide dynamic range gamma-ray spectroscopy with the AGATA detector. *Nuclear Science, IEEE Transactions on*, 56:2384 – 2391, 2009.
32. G. Pascovici, et al. Low noise, dual gain preamplifier with built in spectroscopic pulser for highly segmented high-purity germanium detectors. *WSEAS Trans. Cir. and Sys.*, 7(6):470–481, 2008.
33. The Lund/LBNL table of isotopes. `http://nucleardata.nuclear.lu.se/toi/`.
34. L. Arnold, et al. TNT Digital Pulse Processor. In *14th IEEE-NPSS Real Time Conference, 2005.*, pages 265–269. 2005.
35. V. Jordanov, et al. Digital techniques for real-time pulse shaping in radiation measurements. *Nuclear Instruments and Methods in Physics Research Section A: Accelerators, Spectrometers, Detectors and Associated Equipment*, 353(1):261 – 264, 1994.
36. A. Georgiev, et al. An analog-to-digital conversion based on a moving window deconvolution. *IEEE Transactions on Nuclear Science*, 41(4):1116–1124, 1994.
37. C. D. Unsworth. *Characterisation of an Asymmetric AGATA Detector*. Ph.D. thesis, University of Liverpool, 2011.
38. P. A. Soederstroem, et al. Interaction position resolution simulations and in-beam measurements of the AGATA HPGe detectors. *Nuclear Instruments and Methods in Physics Research Section A: Accelerators, Spectrometers, Detectors and Associated Equipment*, 638(1):96 – 109, 2011.